Urol Res (2011) 39:327–338
DOI 10.1007/s00240-010-0360-8

ORIGINAL PAPER

Cooperation of phosphates and carboxylates controls calcium oxalate crystallization in ultrafiltered urine

Bernd Grohe · Brian P. H. Chan · Esben S. Sørensen · Gilles Lajoie · Harvey A. Goldberg · Graeme K. Hunter

Received: 21 June 2010 / Accepted: 30 December 2010 / Published online: 14 January 2011

Abstract Osteopontin (OPN) is one of a group of proteins found in urine that are believed to limit the formation of kidney stones. In the present study, we investigate the roles of phosphate and carboxylate groups in the OPN-mediated modulation of calcium oxalate (CaOx), the principal mineral phase found in kidney stones. To this end, crystallization was induced by addition of CaOx solution to ultrafiltered human urine containing either human kidney OPN (kOPN; 7 consecutive carboxylates, 8 phosphates) or synthesized peptides corresponding to residues 65–80 (pSHDHMDDDDDDDDGD; pOPAR) or 220–235 (pSHEpSTEQSDAIDpSAEK; P3) of rat bone OPN. Sequence 65–80 was also synthesized without the phosphate group (OPAR). Effects on calcium oxalate monohydrate (COM) and dihydrate (COD) formation were studied by scanning electron microscopy. We found that controls form large, partly intergrown COM platelets; COD was never observed. Adding any of the polyelectrolytes was sufficient to prevent intergrowth of COM platelets entirely, inhibiting formation of these platelets strongly, and inducing formation of the COD phase. Strongest effects on COM formation were found for pOPAR and OPAR followed by kOPN and then P3, showing that acidity and hydrophilicity are crucial in polyelectrolyte-affected COM crystallization. At higher concentrations, OPAR also inhibited COD formation, while P3, kOPN and, in particular, pOPAR promoted COD, a difference explainable by the variations of carboxylate and phosphate groups present in the molecules. Thus, we conclude that carboxylate groups play a primary role in inhibiting COM formation, but phosphate and carboxylate groups are both important in initiating and promoting COD formation.

Keywords Calcium oxalate formation · Morphology · Polyanions · Peptides · Osteopontin · Citrate

B. Grohe (✉) · H. A. Goldberg · G. K. Hunter
Department of Dentistry, Schulich School of Medicine and Dentistry, University of Western Ontario, London, ON N6A 5C1, Canada
e-mail: bgrohe@uwo.ca

B. P. H. Chan · G. Lajoie · H. A. Goldberg · G. K. Hunter
Department of Biochemistry, Schulich School of Medicine and Dentistry, University of Western Ontario, London, ON N6A 5C1, Canada

Present Address:
B. P. H. Chan
School of Medicine, Queen's University, Kingston, ON K7L 3N6, Canada

E. S. Sørensen
Department of Molecular Biology, University of Aarhus, 8000 Aarhus C, Denmark

Introduction

Urine is the primary medium for removing water, salts and metabolic end-products from the body. It is often highly supersaturated with respect to a variety of mineral phases, in particular calcium phosphates and oxalates [1]. The presence of crystals in urine is quite common and usually asymptomatic. However, agglomeration of organic and inorganic compounds can result in aggregates too large to be flushed out by urinary flow. Such composites are mostly generated in the upper urinary tract and can, with time, form even larger stone-like objects. These stones lead to severe pain and disability for approximately 10% of the population of Western nations [2].

The majority of kidney stones (~70%) contain calcium oxalate (CaOx) as their primary mineral phase, often in

combination with calcium phosphates, such as brushite or hydroxyapatite. The remainder of stones contains uric acid, struvite (magnesium ammonium phosphate) or cystine [3]. Although both the monohydrate and the dihydrate phase of calcium oxalate can form under the conditions present in urine, calcium oxalate monohydrate (COM) is much more common in kidney stones [4].

Besides crystal-forming ions, the tubular fluid contains compounds that modulate the nucleation, growth and aggregation of crystals as well as their attachment to renal epithelial cells. These compounds may either inhibit calcification or promote plaque and/or stone formation. It is believed that the initial steps for forming a stone are related to defects in the epithelial cell surface and/or lack of proteins or other compounds in urine that would, under healthy conditions, prevent stone formation [4, 5].

Various low-molecular-weight components of urine, notably citrate, act as inhibitors of crystallization [6]. However, it has recently become clear that most of the inhibitory activity in preventing stone formation resides in proteins [7]. These proteins include osteopontin (OPN), Tamm-Horsfall protein, bikunin (inter-α-trypsin inhibitor) and prothrombin fragment 1, all of which have been shown to inhibit CaOx crystal formation and/or aggregation in vitro [5].

An important protein in oxalate stone formation is OPN [8]. The protein contains about 300 amino acids and undergoes extensive post-translational modification (glycosylation, phosphorylation and sulfation) in a species- and tissue-specific fashion [9]. In vitro studies have shown that OPN is a potent inhibitor of COM growth [10] and aggregation [11] and promotes the formation of the calcium oxalate dihydrate (COD) phase rather than the monohydrate phase [12]. However, in contrast to studies in inorganic solutions [12], Ryall and co-workers [13] recently showed that COD grown in urine has cell-binding affinities similar to that of COM.

It has been demonstrated that OPN inhibits the formation of COM in a phosphorylation-dependent manner [14]. Likewise, synthetic phosphopeptides based on OPN sequences were found to be much more potent inhibitors than the corresponding non-phosphorylated peptides [15, 16]. However, using molecular dynamic simulations, Grohe et al. [16] observed that aspartic and glutamic acid, not phosphoserine, are the amino acids in closest contact with the crystal surface. This indicates that carboxylate groups might play a primary role in mediating growth-inhibition processes [16]. Evidence for such a scenario is (1) the presence of an aspartic acid-rich region within the phosphoprotein [17], and (2) the recent findings showing that OPN and poly-L-aspartic acid (poly-asp) are similar in their COM-inhibiting potencies [18]. The fact that poly-asp, like OPN, strongly affects nucleation [14], growth [18] and agglomeration processes [11] and shifts the predominant COM phase to COD [18] supports such a scenario. The abundance of carboxylic acid residues in these polyelectrolytes provides a potential basis for interactions with crystal surfaces, in particular with high-surface-energy crystal edges and the Ca^{2+}-rich {100} face of COM [14, 19, 20].

To understand the roles of aspartic acid and phosphate groups in nucleation and growth processes, it is necessary to quantify rates of crystallization. Very recently, we have determined volumes of COM and COD precipitated in the presence of various polypeptides [18]. It was found that poly-asp with a molecular mass of ~35.7 kDa is only slightly more potent in inhibiting COM crystallization than rat OPN [18], which contains 43 asp residues (nine consecutive) [17]. However, both are, in turn, much stronger inhibitors of COM formation than non-phosphorylated recombinant OPN [18]. Therefore, the number of phosphate groups (approximately 11 in rat OPN [21]) and their location is critical in the protein's ability to inhibit COM crystallization. Grohe et al. [18] explain these differences in COM-inhibiting potencies in terms of hydrophilicities and net negative charges. However, their studies could not uncover the processes which resulted in COD promotion, effected by some OPN isoforms.

In the present study, we have investigated the roles of phosphate and carboxylate groups in the modulation of CaOx crystal formation using synthetic peptides corresponding to two sequences in rat OPN: amino acids 65–80 and 220–235. The former contains the consecutive-asp sequence found in rat OPN and was synthesized in both a phosphorylated (pSHDHMDDDDDDDDGD, referred to below as pOPAR) and a non-phosphorylated version (SHDHMDDDDDDDDGD, OPAR). The second peptide contains 3 of the 29 phosphorylation sites (serine 220, 223, and 232) identified in OPN from rat bone (pSHEpSTEQSDAIDpSAEK; P3) [21]. In addition, human kidney OPN (kOPN) was used as a positive control.

The effects of these peptides on the formation of COM and COD have been studied using ultrafiltered urine as the crystallization medium. This solution still contains low-molecular-weight components, in particular citrate, that compete with the peptides for crystal interaction. To characterize the effects of polyelectrolytes on crystallizing CaOx, we investigated the growth habit (crystal size and shape), number and volume of COM and COD. We found that COM formation was affected most strongly in the presence of acidic and highly hydrophilic polyelectrolytes containing consecutive-asp sequences. The effects on COD formation, however, were controlled by variations in carboxylates and phosphates present in the molecules, such that phosphorylation promotes the formation of COD.

Materials and methods

Urine collection and analysis

For urine collection and treatment, a modification of the protocol by Doyle et al. [22] was followed. Briefly, 24-h urine samples were collected from eight healthy male volunteers with no history of kidney disease. Prior to (24 h) and during collection, no drugs, alcoholic drinks or caffeinated products were consumed. Immediately after collection, each sample was checked for microscopic hematuria (Chemstrip 5L; Roche Diagnostics Corp., Indianapolis, IN, USA; none showed any evidence of blood) and the urine centrifuged at 10,000 rpm ($\sim$9,630$\times g$; Beckman J2-HS; Beckman Fullerton, CA, USA) for 10 min at room temperature ($\sim$22°C). Vacuum filtration through pre-sterilized filters (pore size: 0.2-μm; Nalgene, Nalge Nunc International, Rochester, NY, USA) into sterile collection bottles (Nalgene) was used for sterilization. There were no preservatives added. To monitor precipitation and sample contamination, the samples were kept at 4°C for a 14-day observation period. After 14 days, approximately two-thirds of the collected urine showed no precipitation. Contamination by bacteria, etc., was never detected (by eye). These samples were pooled, filtered again into sterile bottles and stored at 4°C until experimentation. All filtration procedures were performed in a laminar-flow hood (Microzone H5-MW-99-035; Microzone, Nepean, Canada) to prevent sample contamination.

Chemical analysis of the pooled urine was performed at London Health Sciences Centre (University Hospital London, ON, Canada) using inductively coupled plasma mass spectrometry (ICP-MS; Finnigan Mat, Waltham, MA, USA) and potentiometry for detecting elements as well as spectroscopic methods, such as oxalate-oxidase spectrophotometry, for the determination of molecules.

The University of Western Ontario Research Ethics Board for the Review of Health Sciences Research involving Human Subjects approved the studies. All volunteers gave their informed consent prior to their inclusion in the study.

Chemicals and reagents

Analytical grade calcium nitrate tetra-hydrate ($Ca(NO_3)_2 \cdot 4H_2O$; Sigma-Aldrich, Steinheim, Germany) and sodium oxalate ($Na_2C_2O_4$; EM Science, Gibbstown, NJ, USA) were used as obtained.

Three 16-mer peptides were manually synthesized with free amino and carboxy termini using Fmoc chemistry by a batch method as previously described [16]. Purification of the peptides was achieved by high-performance liquid chromatography on a C18 column and their masses were obtained from electrospray ionization mass spectrometry (ESI-MS; theoretical values in parentheses): P3, 1,972.29 (1,972.64) g/mol; OPAR, 1,833.29 (1,833.60) g/mol; and pOPAR, 1,913.13 (1,913.58) g/mol. Kidney OPN (kOPN) was purified from human urine as described by Christensen et al. [23] and a M_W of 37,700 g/mol was determined by MALDI-TOF mass spectrometry (MALDI-TOF MS; Applied Biosystems). Dephosphorylation of kOPN by alkaline phosphatase revealed a mass loss of 600 g/mol, corresponding to approximately eight phosphate groups distributed over the 30 potential phosphorylation sites [23]. Amino acid analysis (Advanced Protein Technology Centre, Hospital for Sick Children, Toronto, Canada) of the peptides and OPN was carried out using CMC (5-carboxymethylcysteine) as an internal standard to determine the yields.

Solution preparation

For crystallization experiments, inorganic stock solutions of 21.6 mM calcium nitrate and 4.81 mM sodium oxalate were prepared. Deionized water purified with a Milli-Q water system (Millipore Systems, Billerica, MA, USA) and filtration through a 0.2-μm pore-size membrane was used for the preparation of solutions. The pH values of the calcium and the oxalate stocks were 6.04 and 7.39, respectively.

Prior to experimentation, urine from pooled samples was ultrafiltered through Amicon Ultracel filter tubes (Millipore Systems) with a 3,000 molecular weight cut-off by centrifugation at 4,000 rpm ($\sim$3,220$\times g$) for 60 min at 4°C (Eppendorf Centrifuge 5810R; Eppendorf, Hamburg, Germany). If necessary, the pH was adjusted to 5.85 using 5 M hydrochloric acid (analytical grade, Sigma-Aldrich).

Stock solutions of 50 μg/ml peptide or protein (OPAR, pOPAR, P3, kOPN) in ultrafiltered urine were prepared and used for the experiments described below.

Crystallization experiments

Crystallization of CaOxs was carried out by a modification of the method previously described [20]. In brief, crystallization was initiated by adding 1-ml aliquots of preheated (37 ± 0.2°C) urine (800 μl), oxalate (50 μl) and calcium (150 μl) stock solutions to preheated (37 ± 0.2°C) wells of tissue-culture plates (24-well, FALCON, Becton-Dickinson; Franklin Lakes, NJ) containing freshly cleaved mica disks (diameter: 9.5 mm, V-1 grade, SPI® Supplies, Toronto, Canada). The order of addition was oxalate, followed by urine and calcium solutions. If urinary stock solution of OPAR, pOPAR, P3 or kOPN (also preheated) was added to the wells, the volume of urine was correspondingly reduced. Final calcium and oxalate concentrations were 4.7 and

Table 1 Compounds found in urine and corresponding analytical techniques used

Element/molecule	Analysis technique	Concentration measured (mM)	Concentration literature (mM)[a]
Calcium	ICP-MS	1.820 ± 0.066	2.686 ± 1.325
Oxalate	Spectrophotometry[(a)]	0.264 ± 0.006	0.323 ± 0.132
Citrate	Spectrophotometry[(b)]	1.266 ± 0.103	1.396 ± 1.132
Phosphorus	Spectrophotometry[(c)]	19.266 ± 0.398	17.305 ± 6.748
Sulfur	ICP-MS	16.283 ± 0.581	n.a.
Sodium	ICP-MS	99.166 ± 0.983	102.0 ± 44.0
Potassium	Potentiometry	39.000 ± 0.000	29.6 ± 12.8
Chloride	Potentiometry	91.333 ± 0.516	n.a.
Magnesium	ICP-MS	2.220 ± 0.084	2.341 ± 0.999
Boron	ICP-MS	0.088 ± 0.004	n.a.

Values given are mean ± standard deviation (from 6 replicates each): Spectrophotometry of (a) oxalate oxidase, (b) citrate lyase, (c) ammonium molybdate

[a] 133 individuals evaluated: non-pooled urine [33], *n.a.* not available

0.45 mM, respectively. These concentrations are in the ranges of those found in urine of healthy and stone-forming individuals (male or female) [24]. After incubation at 37 ± 0.2°C for 180 min, the mica disks were rinsed with deionized water, air-dried and stored for further investigation. Three replicates were performed for each concentration of each peptide or protein used.

For some representative reactions, pH measurements were carried out immediately after mixing the reaction solutions. The pH was always between 5.8 and 5.9, and well within physiological ranges of healthy and stone-forming individuals [24, 25]. Even high polyelectrolyte concentrations (up to 200 μg/ml) did not significantly affect the pH.

Microscopy and data processing

Scanning electron microscopy (SEM; A LEO 1540XB, Carl Zeiss, Germany) was employed to investigate the precipitates on mica substrates without metal coating, using an acceleration voltage of 1 kV and a working distance of 3.5 mm.

Imaged crystal phases, morphologies and shapes (habits) were evaluated as previously described [18, 26], using crystallographic data (morphologies, crystal symmetry, angles between crystal faces, etc.) available from literature [19, 27–31] and a calculation routine [32]. X-ray diffraction analyses were not performed.

To calculate precipitate volumes, COM and COD crystals were identified, counted and dimensions measured from SEM micrographs as previously described [18]. The individual mean values (±standard deviation) were determined from 6 to 9 microscopic fields (2–3 from each sample) per calculated volume, with between 50 and 350 crystals per microscopic field. One-way ANOVA and Dunnett multiple comparison tests were carried out to test if sample values were significantly different from corresponding controls.

Results

Urine analysis

The more abundant elements and molecules found in the pooled urine samples are listed in Table 1. All concentrations are well within the concentration ranges found in urine of healthy individuals. Besides the compounds indicated in the table, ICP-MS detected the trace elements zinc (~4.6 μM), strontium (~1 μM), selenium (~1 μM), molybdenum (~0.5 μM), iron (~0.2 μM), copper (~0.1 μM), manganese (~4.4 nM), tin (~3.6 nM), cobalt (~2.8 nM), chromium (~2.4 nM) and vanadium (~1.1 nM).

Crystallization under control conditions

Crystallization was initiated by addition of oxalate (50 μl) and calcium (150 μl) solutions to ultrafiltered urine (800 μl). Thus, concentrations of ions and molecules present in urine decreased by a factor of 1.25, except for calcium and oxalate, whose concentrations were increased to 4.7 and 0.45 mM, respectively. However, concentrations of all compounds remained within physiological ranges [24, 33]. The supersaturation σ of CaOxs precipitating in these mixtures is defined as

$$\sigma = 1/2 \ln[(a_{Ca}a_{Ox})/K_{SP}] \quad (1)$$

where K_{SP} is the solubility product for COM ($K_{SP;COM} = 2.24 \times 10^{-9}$ M^2) or COD ($K_{SP;COD} = 6.76 \times 10^{-9}$ M^2) at 37°C [34]. Calculating the activities a by

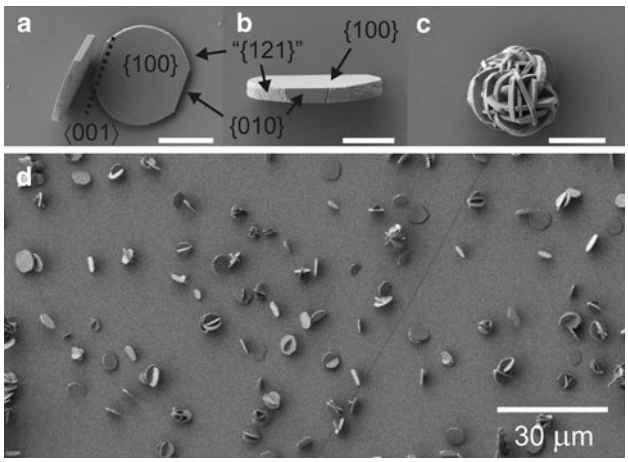

Fig. 1 Scanning electron micrographs (SEM) of COM formed in ultrafiltered urine. **a** Plate-like COM crystals viewed perpendicular (*left*) and parallel (*right*) to a ⟨100⟩ direction. **b** COM crystal viewed from an ⟨010⟩ direction. **c** Interwoven COM platelets. **d** Overview of precipitated calcium oxalate, showing individual and intergrown COM nucleated from all crystal faces developed. *Scale bars* in **a**, **b**, **c**: 3 µm

successive approximation of the ionic strength (see Table 1 except for $[Ca^{2+}] = 4.7$ mM and $[C_2O_4^{2-}] = 0.45$ mM) via the Debye Hückel theory [35] (modified by Davis [36]), supersaturations of 3.33 for COM and 2.78 for COD were determined.

All crystals formed under these conditions appear to be COM. Other crystalline or amorphous phases were not detected. As shown in Fig. 1a and b, COM crystals grown on mica disks are thin and plate-like with well-facetted {100} and {010} crystal planes but rounded faces at both ends of the crystal, a result most likely due to the presence of citrate in urine [28]. In contrast, penetration twins formed in inorganic solutions (controls) grow wider in {100} direction and exhibit well-facetted {121} planes at both crystal ends [18]. We suggests, therefore, that citrate is affecting growth of {100} and {121} faces in ultrafiltered urine. It is, however, not clear in which direction inhibition is strongest and if {010} faces are affected by citrate as well. Some of these crystals are intergrown into each other (Fig. 1d), whereas a few of them grew to aggregates of "interwoven" crystals (Fig. 1c). These aggregates look similar to those found in kidney stones of patients with primary hyperoxaluria [37].

Crystallization in the presence of polyelectrolytes: competition reactions

Effects on crystal habit and morphology

Among the four effectors tested, the phosphopeptide P3 showed the weakest effects on CaOx crystallization. Addition of P3 (≤10 µg/ml) results in COM shapes different from those formed under control conditions (compare Fig. 2a, b with 1a, b). The crystals found are smaller in their ⟨001⟩ and ⟨010⟩ dimensions, show rougher surfaces and are rarely observed at higher P3 concentrations (≥30 µg/ml). The surface roughness appears to be a result of secondary {100} nucleation and growth of COM, a phenomenon, however, not distinctive at P3 concentrations ≥20 µg/ml (Fig. 2c, d). Nucleation of COM occurs from different faces (preferably from {100}) and, besides the {100} faces, all edges are rounded, making indexing the faces difficult. The tendency of COM to intergrowth is strongly decreased in the presence of P3 and abolished at concentrations ≥10 µg/ml (not shown). Addition of P3 also initiates COD formation. The bipyramidal crystals exhibit slightly uneven surfaces (Fig. 2a, d), probably resulting from material deposition or zonal crystal growth, and their dimensions do not significantly change at high effector concentrations (≥10 µg/ml; Fig. 3a). The number of COD crystals nucleating from {100} or {110} crystal planes increases with increasing P3 addition (not shown), a phenomenon probably related to P3 adsorbed to mica acting as receptor for COD nucleation. Some crystals are shown in Fig. 2d.

In the presence of 1–2 µg/ml kOPN, crystallization of COM is strongly decreased and crystal platelets are formed that have some similarities to those induced by P3 (Fig. 2g). Like P3-generated COM, nucleation occurs from all crystal faces (not shown). However, kOPN-formed COM platelets are smaller (∼1/3 of P3-affected ⟨001⟩-direction growth), exhibit edges even more rounded than those formed by P3 and have circular shapes rather than oval shapes (compare Fig. 2g with b, c). Although these shapes allow accurate indexing only for {100} faces, the crystal habits show that growth parallel to ⟨001⟩ is more affected than it is by P3. Moreover, intergrowth of COM and secondary processes are entirely suppressed by the protein, even at concentrations as low as 1 µg/ml (not shown). An example is given in Fig. 2g. At kOPN concentrations ≥2 µg/ml, crystallization of COM is strongly decreased and COD formation dominates the precipitation (Fig. 2e, h). The crystals exhibit bipyramidal shapes, exhibit slightly uneven surfaces (Fig. 2f, i) and become, in contrast to P3-induced COD, smaller at elevated kOPN concentration (>20 µg/ml, Fig. 3b). Higher concentrations (≥30 µg/ml) additionally induce the formation of {100} faces (Fig. 2i). Like crystallization in the presence of P3, increased kOPN concentrations promote COD nucleation from {100} or {110} crystal planes (compare Fig. 2e and h; black arrows). Magnifications of {100}-nucleated COD crystals are shown in Fig. 2i. An example of {110} nucleation is given in Fig. 2d.

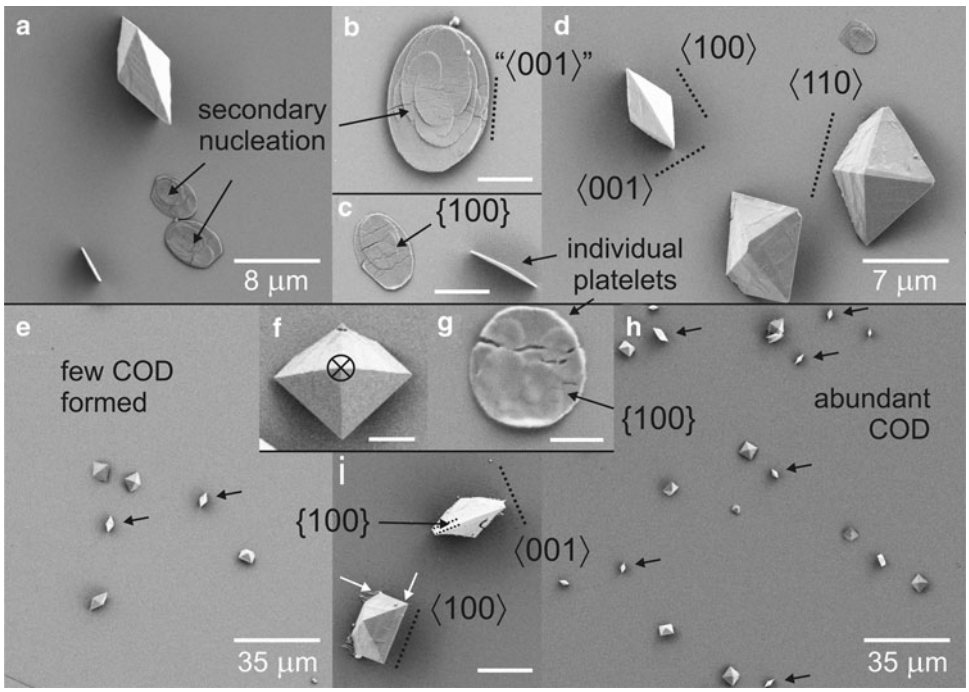

Fig. 2 SEM of COM and COD grown in ultrafiltered urine and in the presence of P3 or kOPN: **a**–**d** P3, **e**–**i** kOPN. Low P3 additions (5 µg/ml P3): oval COM platelets (with **a** secondary nucleation or **b** spiral growth) and COD (bipyramids). **c**, **d** Higher P3 additions (30 µg/ml P3): oval COM platelets (reduced secondary nucleation) and COD nucleated from different crystal planes. Low kOPN additions (2 µg/ml kOPN)—**e** overview: moderate COD formation (*black arrows*: {100} and {110} nucleation), **f** close-up: COD formed with no face specificity (⊗: ⟨001⟩ axis), **g** circular COM platelet. Higher kOPN additions (30 µg/ml kOPN)—**h** overview: abundant COD (*black arrows*: some crystals showing {100} and {110} nucleation), **i** close-up: COD with developed {100} faces (*top*) and with slight effects on growth of edges (*bottom*, *white arrows*). The scale bars in **b**, **c**, **f**, **g** and **i** are 1.82, 2.39, 3.5, 0.76 and 4.45 µm, respectively

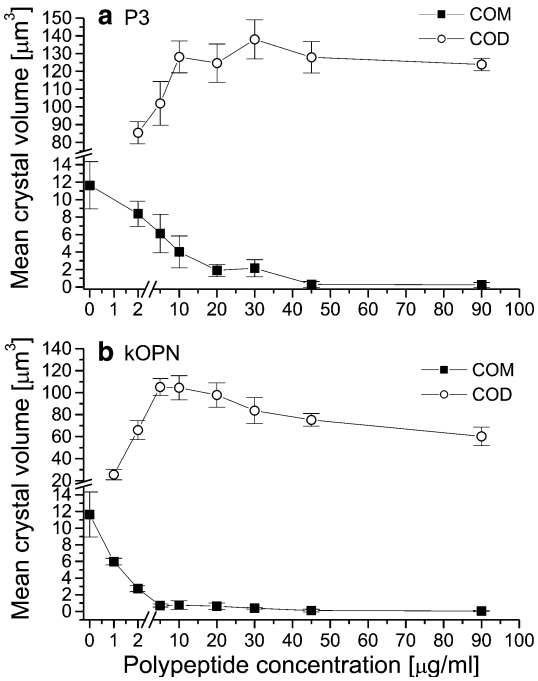

Fig. 3 Mean crystal volume of COM and COD grown in the presence of **a** the phosphopeptide P3 and **b** human kidney OPN

Addition of the aspartic acid-rich peptide OPAR showed effects on COM crystallization very similar to those mediated by kOPN. Precipitation of COM is strongly decreased in the concentration range 0.5–2 µg/ml (at >2 µg/ml, COM is rarely detected) and results in the formation of individual crystal platelets nucleated from different faces (not shown); intergrowth or secondary nucleation and growth of these platelets are not observed (Fig. 4a, b). However, in contrast to kOPN, crystal platelets formed by OPAR are oval-shaped (compare Figs. 4b and 2g) and approximately ∼1/2 the size of P3-crystallized COM (compare Figs. 4b and 2a, b). Compared to P3 and kOPN, lower concentrations are needed to decrease the dimensions of COM platelets drastically (Fig. 5a). The presence of OPAR strongly promotes the precipitation of COD but decreases its formation at higher concentrations (see below). As the mean volume of individual crystals is nearly constant at concentration ≥2 µg/ml (Fig. 5a), nucleation must be inhibited at higher concentration ranges. The crystals exhibit slightly uneven surfaces (similar to the one depicted in Fig. 4a) and show nucleation from {100} or {110} faces (the latter less frequent) when OPAR concentrations are increased (≥30 µg/ml, Fig. 4c, d). Figure 4c shows a close-up of a

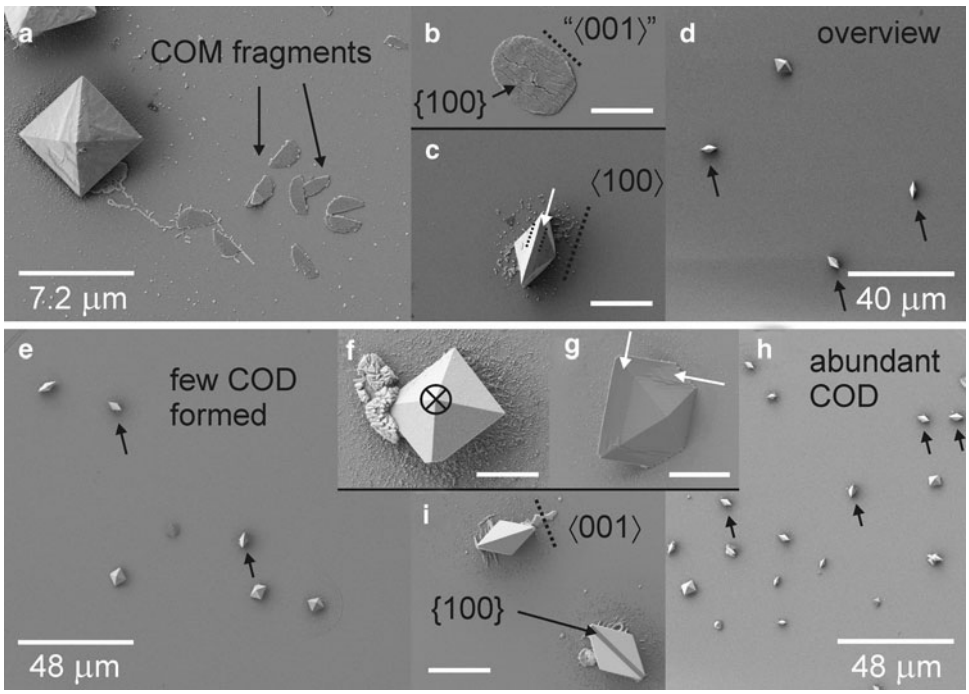

Fig. 4 SEM of COM and COD grown in ultrafiltered urine and in the presence of OPAR or pOPAR: **a**–**d** OPAR, **e**–**i** pOPAR. **a**, **b** Low OPAR additions (2 µg/ml OPAR): individual COM platelets (oval shapes) and fragments are formed, COD formation. Higher OPAR additions (30 µg/ml OPAR)—**c** close-up: slightly affected growth of COD edges (*white arrow*), **d** overview: moderate COD formation from different crystal faces (*black arrows*: {100} and {110} nucleation). Low pOPAR additions (2 µg/ml pOPAR)—**e** overview: COD formation (*black arrows*: {100} and {110} nucleation), **f** close-up: COD nucleated with no distinct face specificity besides some debris (⊗: ⟨001⟩ axis). **g** Moderate pOPAR additions (5 µg/ml pOPAR): slight effects on COD edges (*white arrows*). Higher pOPAR additions (20 µg/ml pOPAR)—**i** close-up: COD with developed {100} faces, **h** overview: abundant COD (*black arrows*: some crystals showing {100} and {110} nucleation). The scale bars in **b**, **c**, **f**, **g** and **i** are 1.77, 4.05, 2.28, 3.16 and 4.78 µm, respectively

{100}-nucleated COD. Higher OPAR additions also showed slight effects on edge growth (onset of growth inhibition parallel to ⟨100⟩; Fig. 4c).

Among the four effectors studied, pOPAR, the phosphorylated version of OPAR, showed the strongest effects on COM crystallization. At concentrations as low as 0.5 µg/ml, the peptide abolished COM formation nearly totally and induced COD formation strongly (Fig. 4e). Additions ≤2 µg/ml form COD of bipyramidal shape with smooth surfaces (Fig. 4f), whereas higher concentrations (≥5 µg/ml) promote COD formation (compare Fig. 4e and h), inhibit COD growth in ⟨100⟩ directions (Fig. 4g, i; crystals exhibit smooth or slightly uneven surfaces), and favor COD nucleation from {100} or {110} crystal planes (Fig. 4h, i; black arrows), although {110} nucleation was observed less frequently. Some {100}-nucleated crystals are shown in Fig. 4i. These effects are initiated at concentrations lower than those used for kOPN or OPAR, suggesting that pOPAR is highly potent in acting as a receptor for COD nucleation on mica substrates. On the other hand, high pOPAR concentrations (>20 µg/ml) are necessary to cause effects on COD dimensions (Fig. 5b).

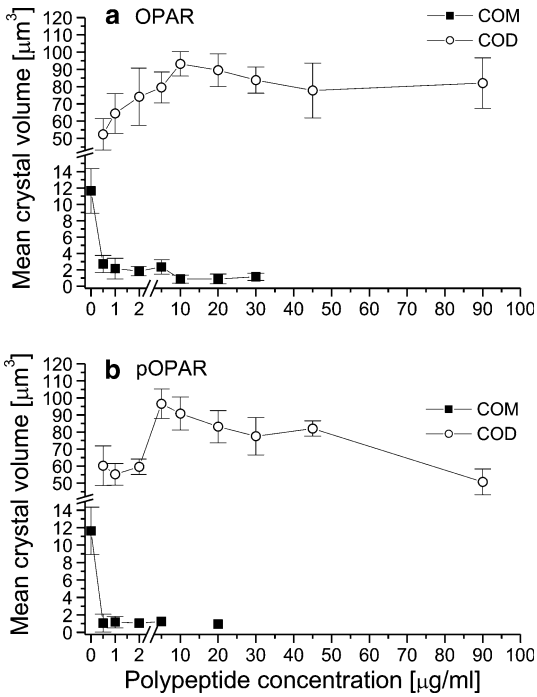

Fig. 5 Mean crystal volume of COM and COD grown in the presence of **a** OPAR and **b** pOPAR

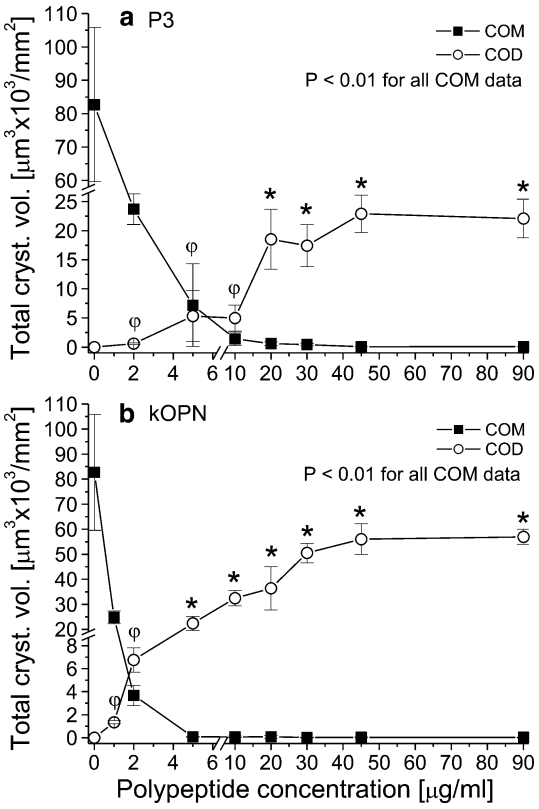

Fig. 6 Crystallization of COM and COD in the presence of **a** the phosphopeptide P3 and **b** human kidney OPN. $^{*}P < 0.01$, significantly different from corresponding control (calculated by Dunnett's multiple comparison test; $^{\varphi}P > 0.05$, not significant)

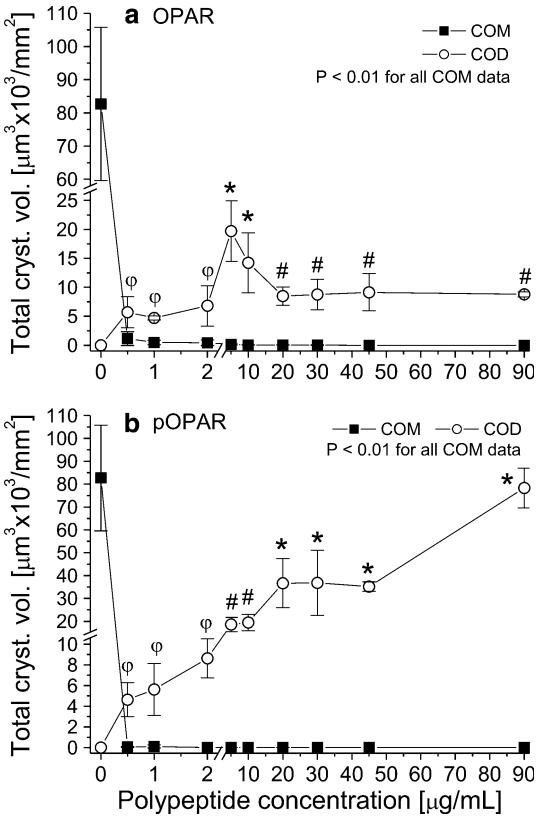

Fig. 7 Crystallization of COM and COD in the presence of different **a** OPAR and **b** pOPAR. $^{\#}P < 0.05$, $^{*}P < 0.01$, significantly different from corresponding control (calculated by Dunnett's multiple comparison test; $^{\varphi}P > 0.05$, not significant)

Effects on precipitation

Using P3, the total crystal volume (TCV; COM plus COD) was smallest at 10 μg/ml, with ~1,400 μm³/mm² of COM (1.71% of COM of controls) and ~5,000 μm³/mm² of COD crystallized (Fig. 6a). However, 45 μg/ml P3 was needed to decrease the COM precipitation rate (nucleation plus growth) to the very low level of ~100 μm³/mm².

In the presence of kOPN, the minimum TCV is reached at 2 μg/ml, with ~3,700 μm³/mm² COM (4.45% of control) and 6,700 μm³/mm² COD (Fig. 6b). Addition of 5 μg/ml kOPN is sufficient to decrease the level of precipitated COM under 100 μm³/mm² and raise COD formation to ~22,000 μm³/mm². The latter finding shows that kOPN has a much stronger dose–response relationship with COD formation than P3 does, abolishing COM formation totally at concentrations ≥5 μg/ml while COD formation is promoted. P3 shows this effect at concentrations ≥45 μg/ml.

Addition of 1 μg/ml OPAR is sufficient to reach a minimum TCV at a level of ~50 μm³/mm² COM (0.06% of control) and ~4,700 μm³/mm² COD (Fig. 7a). This shows that OPAR is more effective than P3 and kOPN in modulating COM and COD formation. However, in contrast to P3 and kOPN, a biphasic dose–response relationship is noted for COD formation. Increasing OPAR concentrations (0–5.0 μg/ml) significantly increase the volume of COD (COM formation is inhibited and, finally, abolished), whereas higher additions (>5.0 μg/ml) increasingly inhibited COD formation.

Effects of pOPAR on CaOx precipitation are shown in Fig. 7b. Obviously, the phosphorylated version of OPAR affects CaOx precipitation most strongly. Addition of 0.5 μg/ml pOPAR results in the smallest TCV found in this work, with ~50 μm³/mm² of COM and 4,600 μm³/mm² of COD crystallized. However, pOPAR is not much more potent than its non-phosphorylated counterpart. Both effectors produce similar minimum TCVs at only slightly different concentrations (0.5 vs. 1.0 μg/ml). Unlike OPAR, however, increasing pOPAR concentrations (≥0.5 μg/ml) result in a promotion of COD formation similar to P3 (≥45 μg/ml) and kOPN (≥5 μg/ml), although COM is totally abolished.

Discussion

The objective of this study was to investigate the effect of OPN and its peptides on the formation of COM and COD

in ultrafiltered urine (pH 5.85). Under the conditions used, CaOx crystals are positively charged [38], whereas the polypeptides tested (kOPN, P3, OPAR, pOPAR) exhibit a net negative charge [18].

Crystallization was performed under non-turbulent and diffusion-controlled conditions (unstirred solutions), in which precipitation (nucleation, growth, phase transformation) is affected by surfaces, effectors, supersaturation, etc. These conditions were chosen as they are more physiological than stirred conditions [39, 40]. Indeed, previous investigations have shown that agitation induces non-physiological aggregation [41, 42] and crystal morphologies [40, 43].

The peptide and protein concentration range chosen (0.5–90 μg/ml) extends well beyond the physiological range (1.9–4.3 μg/ml OPN, with ~4 mg excreted per day [44]). These super-physiological concentrations were studied because of the potential of using OPN peptides as a possible means of treating stone disease in the future.

CaOx crystallization in urine

After ultrafiltration, urine still contains protein fragments (<3 kDa) and low-molecular-weight compounds such as citrate (see Table 1) that compete in modulating CaOx crystallization processes. In the presence of these effectors, COM forms plate-shaped crystals with rounded end faces (Fig. 1a, b), a process reported to be indicative of citrate–COM interactions in aqueous environments [28]. Confirming these results, Qiu et al. [45] observed much stronger interactions of citrate with steps on the most growth-inhibited {100} face than with steps on the weakest affected {010} face and found an explanation for this behavior in electrostatic repulsion. Adsorption to the oxalate-rich {010} face is much less favorable than to the calcium-rich {100} face [19]. However, in contrast to COM platelets found in urine [29], pure aqueous solution–citrate systems form platelets with less rounded and more facetted end faces (in ⟨001⟩ directions), also exhibiting secondary growth processes on {100} faces [28]. As these features are missing in COM of the current study (see Fig. 1a, b), protein fragments are believed to "assist" citrate in modulating step growth on {100} faces. Such a "cooperation" might have promoted the formation of more rounded end faces and smooth {100} crystal planes, lacking any secondary crystallization or spiral growth.

The absence of large proteins (>3 kDa) gives rise to reaction conditions which allow for crystallization of high volumes of COM (see Figs. 6, 7), unhindered intergrowth of COM and the absence of any COD (see Fig. 1). It has been reported that such conditions would be critical with regard to stone formation [5]. Moreover, the plate-like COM crystals formed show substantial similarities to the COM platelets stacked within kidney-stone matrices [30, 39]. Moreover, some of these platelets form interwoven aggregates, which resemble those found in stones of individuals with primary hyperoxaluria [37].

Effects of P3 on CaOx crystallization in urine

Crystallization in the presence of P3 results in growth inhibition of COM in all principal crystallographic directions (compare Fig. 1 with 2a–d). Even {010} faces are affected by P3 interactions with COM. However, the roughness of {100} faces, which is based on secondary nucleation and growth (see Fig. 2b), does not completely disappear, even at higher P3 concentrations (≥30 μg/ml, Fig. 2c). Thus, P3 is a potent growth inhibitor, but it is not potent enough to completely suppress secondary processes. The occurrence of such processes indicates a strong but limited ability of the phosphopeptide to inhibit nucleation of COM, a finding also observed in inorganic solutions [16]. This conclusion finds additional support in the relatively high concentrations needed to abolish COM formation (≥45 μg/ml, Fig. 6a).

An interesting property of P3 is its potency in preventing COM crystals from generating aggregates or from growing together. This outcome is most likely due to the peptide's ability to suppress secondary processes and, therefore, to avert coalescence of crystals. Like inhibition of growth, suppression of coalescence is based on the adsorption of P3 to COM {100} faces [16]. Studies have shown that P3 adsorbs quickly and at early stages of crystallization [46]. At these higher adsorptions rates, P3 is believed to form films that coat the crystals, which, due to electrostatic and/or steric interactions, help to keep COM disaggregated.

COD formation is linked to the inhibited precipitation of COM (see Fig. 6a). Hindered COM crystallization results in a retarded reduction of supersaturation and, therefore, to a higher probability of inducing precipitation of other CaOx phases. As COD is less soluble than calcium oxalate trihydrate [34], the conditions are most favorable for COD formation. Once formed, these crystals are stable, not showing any sign of dissolution during the study. This finding is related to (1) the time needed for dissolving COD [it was found that COD is stable for up to 300 min in supersaturated ($[Ca^{2+}] = [C_2O_4^{2-}] = 2$ mM) inorganic solution; B. Grohe, G. K. Hunter, unpublished data] and (2) P3 adsorption, which, like other strongly binding compounds [47], hinders crystal dissolution. At higher P3 concentrations (≥5 μg/ml), formation of COD is increasingly promoted and a preferred nucleation from {100} or {110} crystal planes is observed, when concentrations exceed ≥20 μg/ml. This behavior is probably related to the adsorption of P3 to mica substrates promoting COD nucleation, a phenomenon also observed when COD

precipitates in the presence of poly-asp in aqueous solution [26] or at epithelial cell surfaces in urine [31]. These findings also indicate that high polyelectrolyte concentrations could promote kidney stone formation, as COD becomes more adhesive to kidney cells [48] or to pre-existing aggregates [30].

Effects of kidney OPN on CaOx crystallization

CaOx precipitation is much more strongly affected by kOPN than by P3. At concentrations as low as 1–2 μg/ml, the protein produces more rounded COM platelets, prevents intergrowth and secondary growth of COM and induces COD formation strongly (Fig. 2e–i). The formation of circular habits shows that COM growth parallel to ⟨001⟩ is more strongly affected than it is by P3. Moreover, the crystal platelets formed are smaller and thinner (parallel to ⟨100⟩) than those induced by the phosphopeptide. These findings suggest that kOPN preferentially adsorbs to {100} faces and to step risers of {121} and {021} steps at {100} faces, a process provoking strong growth inhibition parallel to ⟨100⟩ and ⟨001⟩ of just-nucleated crystals. Even {010} faces are more strongly affected by kOPN than by P3. In inorganic solutions, OPN has been shown to adsorb selectively to {121}/{100} edges of pregrown COM [20] and, when present at concentrations ≥1 μg/ml, also to {100} faces [49]. The same studies and investigations by Langdon et al. [14] have reported preferred inhibition of COM growth parallel to ⟨001⟩ and effects of the protein on all other crystallographic directions. Moreover, growth inhibition was observed as soon as crystals formed indicating fast adsorption of the protein to crystallizing COM [14]. However, these processes all resulted in dumbbell-like habits. Pancake morphologies like those found in the present study were not observed. This outcome suggests that cooperative effects of kOPN, citrate, protein fragments and other compounds modulate COM crystallization much more strongly than does kOPN alone. The fact that ∼5 μg/ml kOPN is sufficient to nearly extinguish COM (Fig. 6b) supports such a scenario for ultrafiltered urine.

Strong binding of OPN might also explain the lack of any crystal aggregates. At concentrations ≥0.2 μg/ml, OPN has been shown to adsorb to all faces of COM and form protein aggregates at crystal surfaces [50]. These aggregates not only decrease the flux of lattice ions to the crystal surface, thereby hindering growth of COM, but also block secondary COM formation at crystal surfaces and favor a steric repulsion in particle–particle interaction [51]. Characteristics such as the size of the protein (compared to e.g. P3), its conformation when adsorbed to COM, the number and distribution of hydrophilic and hydrophobic residues, etc., may have contributed to the observed effects on COM formation.

COD crystallization strongly depends upon the presence and concentration of kOPN. At lower protein concentrations (up to 5 μg/ml), precipitation is characterized by suppression of COM and promotion of COD. However, unlike P3, relatively small concentrations (∼5 μg/ml) of kOPN are sufficient for precipitating COD predominantly (compare Fig. 6a, b). The crystals formed get smaller (Fig. 3b) and more frequent (Fig. 2e, h) at higher kOPN concentrations (>20 μg/ml), a process also observed in inorganic solutions using different OPN isoforms [18]. The latter finding is evidence for an increased nucleation rate, probably induced by decreased activation energies for nucleation during interactions of the crystallizing matter with concentrated protein bound to mica [52].

At high kOPN concentrations (≥20 μg/ml), COD preferentially nucleates from {100} or {110} crystal planes, an effect that was also observed for P3 (see above) and other effectors in urinary or inorganic environments [26, 31]. It is assumed that this effect results from highly concentrated kOPN bound to the substrate surface [50, 52] and the calcium richness of the {100} and {110} COD faces [53, 54]. Moreover, {100} faces not in contact with substratum were also observed, suggesting an effect of kOPN in solution as well (see Fig. 2i). Similar observations are reported by Chien et al. [54] who showed that OPN strongly affects {100} face formation of COD in urine. As modulation of {100} growth was not observed when using OPN in inorganic solutions [18], we assume that kOPN and low molecular compounds cooperatively affect {100} face formation of COD in urine.

Effects of [p]OPAR on CaOx crystallization

The presence of OPAR or pOPAR ([p]OPAR) strongly inhibits COM formation. Concentrations as low as 0.5–1.0 μg/ml are sufficient to suppress COM crystallization nearly totally, with pOPAR being slightly more potent (see Fig. 7a, b). At higher concentrations (≥2 μg/ml), COM was rarely observed. Thus, [p]OPAR has a strong effect on COM nucleation, even stronger than kOPN, suggesting that [p]OPAR interferes very early in cluster formation of the crystallizing matter. This finding also shows that COM inhibition processes are affected strongest by pOPAR and OPAR followed by kOPN and then P3, an order indicating that the acidity and hydrophilicity are the controlling factors in preventing COM crystallization [18].

The COM platelets formed by [p]OPAR show no aggregation or secondary processes (Fig. 3a, b). This implies that [p]OPAR, like kOPN, strongly binds to COM and coats the crystals, which aids COM in staying disaggregated. On the other hand, both the phosphorylated and the non-phosphorylated peptide form oval crystal platelets, suggesting that the adsorption (not inhibition) pattern of

[p]OPAR might be similar to that found for poly-asp (35.7 kDa), which adsorbed non-selectively to all faces of COM when studied in inorganic solution [18]. Taking these findings into account, [p]OPAR is proposed to interact strongly with {100} faces, more weakly with {121} faces and only marginally with {010} faces (probably via Ca^{2+}-bridging to oxalate [50]). Such a scenario could be based on electrostatic peptide–crystal interactions caused by differences in Ca^{2+} ion densities of these crystal faces [19].

COD formation is affected slightly differently by OPAR and pOPAR. In contrast to OPAR, which inhibits COD, there is a continuing increase in COD content with increasing pOPAR concentrations (>5 μg/ml), an outcome also observed for the parent protein and, to a lesser extent, for P3 (compare Figs. 6 and 7). These findings are evidence for a process in which phosphate groups act as mediators of COD nucleation, a process similar to that described for the cooperation of sulfates and carboxylates in calcite crystallization [55]. A combination of phosphate groups and contiguous carboxylate groups (present in kOPN and pOPAR) may result in additional nucleation centers for COD by generating sites at the substrate surface with higher charge densities. When, however, carboxylates are underrepresented or not consecutive, like in P3, COD formation is less promoted. In contrast, the lack of phosphate groups, like in OPAR, results in a biphasic effect on COD formation, a behavior similar to that found for poly-asp in inorganic solutions [18].

Closing remarks

Recently, weakly acidic, basic and/or hydrophobic peptides have been shown to only affect crystallization processes poorly or not at all, even if phosphorylated [15, 16]. Our present study demonstrates, however, that phosphorylated aspartic acid-rich regions of OPN are very potent in inhibiting COM crystal and aggregate formation and promote the formation of the COD phase. Based on these findings, polycarboxylated peptides (probably phosphorylated to control the formation of COD) are very promising agents to assist endogenous inhibitors in preventing initial stone formation and/or reducing recurrence rates.

Acknowledgments The authors thank Todd Simpson (Nanofabrication Facility, Department of Science, University of Western Ontario) for electron microscopy and Yinyin Liao (Department of Dentistry, University of Western Ontario) for expert technical assistance. The studies reported here were supported by the Canadian Institutes of Health Research. B.C. received a Studentship in Musculoskeletal Health from the Institute for Musculoskeletal Health and Arthritis, Canada.

Conflict of interest The authors have no conflicts of interest to disclose.

References

1. Coe FL, Parks JH (1988) Nephrolithiasis: pathogenesis and treatment. Year Book Medical, Chicago, IL, pp 1–37
2. Coe FL, Evan A, Worcester E (2005) Kidney stone disease. J Clin Invest 115:2598–2608
3. Bushinsky DA (2001) Kidney stones. Adv Intern Med 47:219–238
4. Lieske JC, Toback FG (2000) Renal cell–urinary crystal interactions. Curr Opin Nephrol Hypertens 9:349–355
5. Khan SR, Kok DJ (2004) Modulators of urinary stone formation. Front Biosci 9:1450–1482
6. Mattle D, Hess B (2005) Preventive treatment of nephrolithiasis with alkali citrate—a critical review. Urol Res 33:73–79
7. Ryall RL (2004) Macromolecules and urolithiasis: parallels and paradoxes. Nephron Physiol 98:37–42
8. Kleinman JG, Wesson JA, Hughes J (2004) Osteopontin and calcium stone disease. Nephron Physiol 98:43–47
9. Sodek J, Ganss B, McKee MD (2000) Osteopontin. Crit Rev Oral Biol Med 11:279–303
10. Shiraga HM, Min W VanDusen WJ, Clayman MD, Miner D, Terrell CH, Sherbotie JR, Foreman JW, Przysiecki C, Nielson EG, Hoyer JR (1992) Inhibition of calcium oxalate crystal growth in vitro by uropontin: another member of the aspartic acid-rich protein superfamily. Proc Natl Acad Sci USA 89:426–430
11. Asplin JR, Arsenault D, Parks JH, Coe FL, Hoyer JR (1998) Contribution of human uropontin to inhibition of calcium oxalate crystallization. Kidney Int 53:194–199
12. Wesson JA, Worcester EM, Wiessner JH, Mandel NS, Kleinman JG (1998) Control of calcium oxalate crystal structure and cell adherence by urinary macromolecules. Kidney Int 53:952–957
13. Wang T, Thurgood LA, Grover PK, Ryall RL (2010) A comparison of the binding of urinary calcium oxalate monohydrate and dihydrate crystals to human kidney cells in urine. BJU Int 106(11):1768–1774
14. Langdon A, Wignall GR, Rogers KA, Sørensen ES, Denstedt J, Grohe B, Goldberg HA, Hunter GK (2009) Kinetics of calcium oxalate crystal growth in the presence of osteopontin isoforms: an analysis by scanning confocal interference microcopy. Calcif Tissue Int 84:240–248
15. Hoyer JR, Asplin JR, Otvos L (2001) Phosphorylated osteopontin peptides suppress crystallization by inhibiting the growth of calcium oxalate crystals. Kidney Int 60:77–82
16. Grohe B, O'Young J, Ionescu DA, Lajoie G, Rogers KA, Karttunen M, Goldberg HA, Hunter GK (2007) Control of calcium oxalate crystal growth by face-specific adsorption of an osteopontin phosphopeptide. J Am Chem Soc 129:14946–14951
17. Oldberg A, Franzen A, Heinegard D (1986) Cloning and sequence-analysis of rat bone sialoprotein (osteopontin) cDNA reveals an Arg-Gly-Asp cell-binding sequence. Proc Natl Acad Sci USA 83:8819–8823
18. Grohe B, Taller A, Vincent PL, Tieu LD, Rogers KA, Heiss A, Sorensen ES, Mittler S, Goldberg HA, Hunter GK (2009) Crystallization of calcium oxalates is controlled by molecular hydrophilicity and specific polyanion–crystal interactions. Langmuir 25:11635–11646
19. Jung T, Sheng XX, Choi CK, Kim WS, Wesson JA, Ward MD (2004) Probing crystallization of calcium oxalate monohydrate and the role of macromolecule additives with in situ atomic force microscopy. Langmuir 20:8587–8596
20. Taller A, Grohe B, Rogers KA, Goldberg HA, Hunter GK (2007) Specific adsorption of osteopontin and synthetic polypeptides to calcium oxalate monohydrate crystals. Biophys J 93:1768–1777
21. Keykhosravani M, Doherty-Kirby A, Zhang C, Brewer D, Goldberg HA, Hunter GK, Lajoie G (2005) Comprehensive

identification of post-translational modifications of rat bone osteopontin by mass spectrometry. Biochemistry 44:6990–7003
22. Doyle IR, Ryall RL, Marshall VR (1991) Inclusion of proteins into calcium-oxalate crystals precipitated from human urine—a highly selective phenomenon. Clin Chem 37:1589–1594
23. Christensen B, Petersen TE, Sorensen ES (2008) Post-translational modification and proteolytic processing of urinary osteopontin. Biochem J 411:53–61
24. Taylor EN, Curhan GC (2006) Body size and 24-hour urine composition. Am J Kidney Dis 48:905–915
25. Whitson JM, Cooperberg MR, Stackhouse GB, Stoller ML (2007) Urinary citrate levels do not correlate with urinary pH in patients with urinary stone formation. Urology 70:634–637
26. Grohe B, Rogers KA, Goldberg HA, Hunter GK (2006) Crystallization kinetics of calcium oxalate hydrates studied by scanning confocal interference microscopy. J Cryst Growth 295:148–157
27. Millan A (2001) Crystal growth shape of whewellite polymorphs: influence of structure distortions on crystal shape. Cryst Growth Des 1:245–254
28. Shirane Y, Kagawa S (1993) Scanning electron-microscopic study of the effect of citrate and pyrophosphate on calcium-oxalate crystal morphology. J Urol 150:1980–1983
29. Werness PG, Bergert JH, Smith LH (1981) Crystalluria. J Cryst Growth 53:166–181
30. Iwata H, Iio S, Nishio S, Takeuchi M (1992) Architecture of mixed calcium-oxalate dihydrate and monohydrate stones. Scanning Microsc 6:231–238
31. Lieske JC, Toback FG, Deganello S (2001) Sialic acid-containing glycoproteins on renal cells determine nucleation of calcium oxalate dihydrate crystals. Kidney Int 60:1784–1791
32. Data were entered into a calculation routine available in http://www.mathe-formeln.de
33. Pak CYC, Adams-Huet B (2004) Elucidation of factors determining formation of calcium phosphate stones. J Urol 172:2267–2270
34. Königsberger E, Königsberger L-C (2001) Thermodynamic modeling of crystal deposition in humans. J Pure Appl Chem 73:785–797
35. Debye P, Hückel E (1923) The theory of electrolytes. I. Lowering of freezing point and related phenomena. Physikalische Zeitschrift 24:185–206
36. Davis CW (1962) Ion association. Butterworth, London
37. Daudon M, Bazin D, Andre G, Jungers P, Cousson A, Chevallier P, Vernon E, Matzen G (2009) Examination of whewellite kidney stones by scanning electron microscopy and powder neutron diffraction techniques. J Appl Crystallogr 42:109–115
38. Fernandez JC, Delasnieves FJ, Salcedo JS, Hidalgoalvarez R (1990) The microelectrophoretic mobility and colloid stability of calcium-oxalate monohydrate dispersions in aqueous-media. J Colloid Interf Sci 135:154–164
39. Sandersius S, Rez P (2007) Morphology of crystals in calcium oxalate monohydrate kidney stones. Urol Res 35:287–293
40. Kile DE, Eberl DD (2003) On the origin of size-dependent and size-independent crystal growth: influence of advection and diffusion. Am Mineral 88:1514–1521
41. Zauner R, Jones AG (2000) Determination of nucleation, growth, agglomeration and disruption kinetics from experimental precipitation data: the calcium oxalate system. Chem Eng Sci 55:4219–4232
42. Wesson JA, Ganne V, Beshensky AM, Kleinman JG (2005) Regulation by macromolecules of calcium oxalate crystal aggregation in stone formers. Urol Res 33:206–212
43. McCabe WL (1929) Crystal growth in aqueous solutions. Ind Eng Chem 21:30–33
44. Min W, Shiraga H, Chalko C, Goldfarb S, Krishna GG, Hoyer JR (1998) Quantitative studies of human urinary excretion of uropontin. Kidney Int 53:189–193
45. Qiu SR, Wierzbicki A, Salter EA, Zepeda S, Orme CA, Hoyer JR, Nancollas GH, Cody AM, De Yoreo JJ (2005) Modulation of calcium oxalate monohydrate crystallization by citrate through selective binding to atomic steps. J Am Chem Soc 127:9036–9044
46. Wignall GR, Langdon AN, Grohe B, Goldberg HA, Denstedt JD, Hunter GK (2008) Inhibited growth of calcium oxalate monohydrate in the presence of osteopontin and synthetic phosphopeptides. J Urol 179:565–566
47. Sikiric M, Filipovic-Vincekovic N, Babic-Ivancic V, Vdovic N, Furedi-Milhofer H (1999) Interactions in calcium oxalate hydrate surfactant systems. J Colloid Interf Sci 212:384–389
48. Verkoelen CF, van der Boom BG, Kok DJ, Romijn JC (2000) Sialic acid and crystal binding. Kidney Int 57:1072–1082
49. Hunter GK, Grohe B, Jeffrey S, O'Young J, Sørensen ES, Goldberg HA (2009) Role of phosphate groups in inhibition of calcium oxalate crystal growth by osteopontin. Cells Tissues Organs 189:44–50
50. Weaver ML, Qiu SR, Hoyer JR, Casey WH, Nancollas GH, De Yoreo JJ (2009) Surface aggregation of urinary proteins and aspartic acid-rich peptides on the faces of calcium oxalate monohydrate investigated by in situ force microscopy. Calcif Tissue Int 84:462–473
51. Philipse A (2005) Particulate colloids: aspects of preparation and characterization. Elsevier, Amsterdam
52. Zappone B, Thurner PJ, Adams J, Fantner GE, Hansma PK (2008) Effect of Ca^{2+} ions on the adhesion and mechanical properties of adsorbed layers of human osteopontin. Biophys J 95:2939–2950
53. Heijnen WMM, Vanduijneveldt FB (1984) The theoretical growth-morphology of calcium-oxalate dihydrate. J Cryst Growth 67:324–336
54. Chien YC, Masica DL, Gray JJ, Nguyen S, Vali H, Mckee MD (2009) Modulation of calcium oxalate dihydrate growth by selective crystal-face binding of phosphorylated osteopontin and polyaspartate peptide showing occlusion by sectoral (compositional) zoning. J Biol Chem 284:23491–23501
55. Addadi L, Moradian J, Shay E, Maroudas NG, Weiner S (1987) A chemical-model for the cooperation of sulfates and carboxylates in calcite crystal nucleation—relevance to biomineralization. Proc Natl Acad Sci USA 84:2732–2736